SURE 静岡大学学術リポジトリ
Shizuoka University REpository

Advancement of capture immunoassay for real-time monitoring of hepatitis E virus-infected monkey

メタデータ	言語: eng 出版者: 公開日: 2020-02-13 キーワード (Ja): キーワード (En): 作成者: Khoris, Indra Memdi, Chowdhury, Ankan Dutta, Li, Tian-Cheng, Suzuki, Tetsuro, Park, Enoch Y. メールアドレス: 所属:
URL	http://hdl.handle.net/10297/00027057

Advancement of capture immunoassay for real-time monitoring of hepatitis E virus-infected monkey

Indra Memdi Khoris[a], Ankan Dutta Chowdhury[b], Tian-Cheng Li[c], Tetsuro Suzuki[d], Enoch Y. Park[a,b,*]

[a] Department of Applied Biological Chemistry, College of Agriculture, Graduate School of Integrated Science and Technology, Shizuoka University, 836 Ohya Suruga-ku, Shizuoka 422-8529, Japan

[b] Research Institute of Green Science and Technology, Shizuoka University, 836 Ohya Suruga-ku, Shizuoka 422-8529, Japan

[c] Department of Virology 2, National Institute of Infectious Diseases, 4-7-1 Gakuen, Musashimurayam-shi, Tokyo 208-0011, Japan

[d] Department of Infectious Disease, Hamamatsu University School of Medicine, Handayama, Hamamatsu 431-3125, Japan

E-mail:

indra.memdi.khoris.17@shizuoka.ac.jp (IMK)
ankan.dutta.chowdhury@shizuoka.ac.jp (ADC)
litc@nih.go.jp (TCL)
tesuzuki@hama-med.ac.jp (TS)
park.enoch@shizuoka.ac.jp (EYP)

[*] Corresponding author: Research Institute of Green Science and Technology, Shizuoka University, 836 Ohya Suruga-ku, Shizuoka 422-8529, Japan.
E-mail address: park.enoch@shizuokac.jp

Abstract

Rapid increasing outbreak of Hepatitis E virus (HEV) shows an urgent need of HEV detection. Instead of time consuming and expensive RT-qPCR, an efficient and quick monitoring system is in utmost demand which can be comparable with the RT-qPCR in term of reliability and detection limit. An advanced platform for immunoassay has been constructed in this study by a nanozyme that constitutes anti-HEV IgG antibody-conjugated gold nanoparticles (Ab-AuNPs) as core and *in situ* silver deposition on the surface of Ab-AuNPs as outer shell. The virus has been entrapped on the nanocomposites while the silver-shell has decomposed back to the silver ions (Ag^{+}) by adding a tetramethylbenzidine (TMBZ) and hydrogen peroxide (H_2O_2) which indirectly quantifies the target virus concentration. Counterpart to only applying nanozyme, by incorporation of the enhanced effect of Ag shell on the AuNP-based nanozyme, the advance deposition has been confirmed to prove the signal amplification mechanism in the proposed immunoassay. Most importantly, the sensor performances have examined in clinically isolated HEV from HEV-infected monkey over a period of 45 days which successfully correlated with their standard RT-qPCR data, showing the applicability of this immunoassay as a real-time monitoring on the HEV infection. The *in situ* formation of AuNPs@Ag as nanozyme in this capture immunoassay leads to a promising advancement over the conventional methods and nanozyme-based immunoassay in real application which can be a good substitute of RT-qPCR in near future.

***Keywords*:** Colorimetric detection, Gold nanoparticle, Hepatitis E virus, Immunoassay, Nanozyme, Virus sensing

1. Introduction

HEV infection has become a serious health concern due to the increasing outbreak of Hepatitis E in developing as well as developed countries, which are mostly contributed via waterborne and zootomic-transmitted pathway [1]. Hepatitis E is associated to liver failure and acute liver disease, with higher fatality during pregnancy [2, 3]. Recently, major development in HEV detection platform is targeting on the RNA-targeting RT-PCR and antibodies (IgG, IgM and IgA) that were produced after the infection of HEV [4, 5]. Due to the limited available diagnostic assay on HEV, a reliable antigen-targeting immunoassay is required to outstand the emerging outbreak by early detection of the disease agent. Instead of RT-qPCR, enzyme-linked immunosorbent assay (ELISA) has been well-known for its simplicity with step-by-step procedure to determine the presence of the target analyte [6, 7]. Commonly, a colorimetric-based ELISA utilized peroxidase as the enzyme which catalyzes the oxidation of chromogen substrate by hydrogen peroxide. However, its low sensitivity has been addressed as a strong limitation in detecting HEV type of viral agents, where very low concentration of virus can make the fatality [6]. This issue can be addressed by the signal amplification used in the platform [8, 9]. An upgraded ELISA-based biosensor with comparable reliability of RT-qPCR has been in necessity to restrict the outbreak of HEV.

Since the first discovery of Fe_3O_4 nanoparticles (NPs) exhibiting peroxidase-like activity, known as nanozyme, more application with various kind of nanozymes has been discovered, especially in biosensing technology [9-11]. Various applications such as enzymatic activity [12], nanozymes has been shown to either enhance the activity of the coupled enzymes or exhibiting robust enzymatic-like activity [13, 14]. Nanomaterials, especially noble metals, such as gold (Au)[15], silver (Ag)[16] and platinum (Pt)[17], have been employed to substitute the current enzyme used in the immunoassay due to their intrinsic peroxidase-like activity, good stability and biocompatibility [18-21]. Interestingly, hybrid nanomaterial, such as

graphene/gold nanohybrid [22], gold-decorated organic framework [23], and bimetallic [24-27] to trimetallic [28, 29] nanostructure, demonstrated unique morphology and increasing catalytic activity significantly [30]. To achieve the desired specificity, proper bioconjugation has to be applied successfully. However, in contrast, to maintain the specificity of the nanozyme, bioconjugation can reduce its catalytical activity to some extent [20, 31]. To make an optimized condition for modified immunoassays, noble metals have been emerging as a potential platform for easy bioconjugation step with compromising their activity. In this case, Au can be an automatic choice for its less toxicity and cost effectiveness than Pt, and higher plasmonic characteristic compared to Ag in addition with its easy functionalized and control-synthesized properties [32].

In order to develop a highly sensitive nanozyme-based immunoassay for HEV detection, in this study, a signal amplification strategy has been introduced by utilizing silver deposition on Au nanozyme. In our previous study, a proposed immunoassay was demonstrated for norovirus detection and enhanced colorimetric signal in low concentration [20]. Therefore, in this study, more reliable approach was applied to on-site detection and the results were compared to conventional RT-qPCR. However, similar with most of the colorimetric assays, the bare gold nanoparticles (AuNPs) could not be able to perform well in the desired concentration range for real sample analysis. To enhance the performance and stability in real sample medium, in this work, we have proposed a core shell nanocomposite with silver. Silver deposition on gold nanoparticles, was already previously reported for its application in surface-enhanced Raman scattering detection [33], mass spectrometry [34], and opacity densitometry [35], however its applicability is not well explored in the field of catalytic enhancement, especially for virus detection. According to our hypothesis, the AuNPs core with Ag shell structure (AuNPs@Ag) has been introduced for the enhanced catalytic activity of the Ag towards TMB-based color development. The homogeneous distributed AuNPs@Ag with

higher stability have been successfully combined to make an upgraded platform for virus detection, especially for real sample analysis. To establish the mechanism, the AuNPs@Ag nanocomposite was synthesized separately and optimized to get the best suited condition for the detection. Then the system was applied *in situ* deposition during virus-sensing process in the antigen-antibody interaction. A capture immunoassay was demonstrated for HEV detection by using HEV-like particles (HEV-LPs) as the model. By conjugating the Au nanozyme with anti-HEV IgG antibody, the proposed immunoassay demonstrated an amplified signal for low concentration of HEV-LPs. In the presence of silver deposition solution containing silver ions (Ag^+) and hydroquinone (HQ) and chromogen solution containing hydrogen peroxide (H_2O_2) and 3,3',5,5'-tetramethylbenzidine (TMBZ), the color as a detection signal was significantly amplified compared to the bare AuNP system. In the final step, the nanozyme-based capture immunoassay was challenged to detect the viral HEV containing in fecal samples collected from HEV-infected monkey and showed a comparable trend with RT-qPCR, representing its promising application towards the detection of HEV.

2. Materials and methods

2.1 Materials and Instruments

Gold (III) chloride trihydrate ($HAuCl_4 \cdot 3H_2O$), bovine serum albumin (BSA), and silver nitrate ($AgNO_3$) were purchased from Sigma-Aldrich (St. Louis, MO, USA). Tetramethylbenzidine (TMBZ) was purchased from Dojindo (Osaka, Japan). Hydrogen peroxide (H_2O_2), dimethyl sulfoxide (DMSO), hydroquinone (HQ), sulfuric acid (H_2SO_4), detergent tween-20, and sodium acetate (NaAc) were purchased from Wako Pure Chem., Inc. (Osaka, Japan). Anti-IgG rabbit pAb-conjugated to horseradish peroxidase (HRP) antibody was purchased from Santa Cruz Biotechnology (CA, USA). All experiments were conducted using deionized (DI) water.

Morphology of AuNPs and high-resolution images for AuNPs@Ag were conducted by using transmission electron microscope (TEM) (JEM-2100F, JEOL, Ltd., Tokyo, Japan) with voltage at 100 kV and at 200 kV, respectively. Hydrodynamic particle size and zeta potential measurement were carried out using a Malvern Zetasizer (Nano-ZS, Malvern, UK) in a disposable zeta cell (DTS1061).

2.2 Preparation of HEV-LPs, Anti-HEV IgG antibody and HEV

The G3 HEV-LPs were produced by a recombinant baculovirus expression system as described previously [36, 37]. The anti-G3 HEV-LPs IgG antibody obtained from a rabbit which were immunized with purified G3 HEV-LPs, and purified by protein G column [36]. A series of 14 fecal specimens were collected from 4 to 43 day postinfection (dpi) from a G7 HEV-infected cynomolgus monkey. The fecal specimens were diluted with 10 mM in PBS to prepare a 10% (w/v) suspension. Then the suspension was shaken at 4°C for 1 h, clarified by centrifugation at 10,000 × *g* for 30 min, passed through a 0.45 μm membrane filter (Millipore, Bedford, MA), and stored at –80°C until use. All of the HEV samples were inactivated by incubation at 70°C for 20 min before using this study.

For selectivity test, zika virus (PRVABC-59) and fecal norovirus (NoV) were kindly provided by Professor K. Morita of Institute of Tropical Medicine, Nagasaki University and Dr. Fuyuki Abe of Department of Microbiology, Shizuoka Institute of Environment and Hygiene, respectively. Fecal NoV were prepared according to the previous protocol [20]. Influenza virus A/Netherland/H7N7 were purchased from ProSpec-Tany Technogene, Ltd (East Brusnwick, NJ, USA).

2.3 Preparation of Buffer, Silver deposition and Chromogen Solutions

10 × Phosphate-buffered saline (PBS) solution was prepared in following composition; 80 g sodium chloride, 2 g potassium chloride, 11.5 g sodium hydrogen phosphate, and 2 g potassium dihydrogen phosphate in 1 L (pH 7.4). Washing buffer was prepared by mixing 100 mL 1 × PBS (1 M) solution with 0.5 mL 20% Tween-20. Silver deposition solution was prepared by diluting 100 mM $AgNO_3$ and 100 mM hydroquinone (HQ) up to final concentration of 1 mM Ag^+. Chromogen solution in proposed immunoassay was prepared by adding 10 mg/mL TMBZ in DMSO to 30% H_2O_2 in 1:9 v/v. Acetate buffer was prepared by adding 20.4 g sodium acetate trihydrate and 5.7 mL acetic acid, mess up to 50 mL with DI water (pH 5.2). Chromogen solution was prepared by adding 20 µL 10 mg/mL TMBZ in DMSO to 0.2 µL H_2O_2 in 1 mL acetate buffer (pH 5.2). BSA (5%) was used as blocking agent by dissolving it in 1 × PBS. Stop solution was prepared by dilution of H_2SO_4 up to 10%

2.4 Synthesis of Citrate-capped AuNPs and AuNPs@Ag

AuNPs were synthesized by the citrate reduction method [34]. Briefly, 40 mL of 0.5 mM $HAuCl_4 \cdot 3H_2O$ was heated to boiling condition and stirred for 30 min, and then 1 mL of 2% (w/v) trisodium citrate trihydrate was added into the boiling solution. In a short time, the color of the solution changed from pale yellow to colorless, then dark color and gradually to red-wine color. The solution was stirred continuously for an additional 10 min without any heating. The solution was then cooled to room temperature and stored at 4°C. To prepare the AuNPs@Ag, the as-synthesized AuNPs was reacted to $AgNO_3$ (1 mM) and HQ (1 mM) (1:1 v/v) and the solution was mixed and incubated for 15 min with no heating involved. The color change was observable from reddish wine to reddish orange. The resulting mixture was then centrifuged at 8,500 g for 15 min at 7°C. The nanomaterials were stored in 4ºC and showed no color change up to several weeks.

176 *2.5 Bioconjugation of Antibody to AuNPs and ELISA*

177 To conjugate via physical adsorption of the surface of AuNPs with anti-HEV IgG antibody
178 (Ab), final concentration of 10 µg/mL anti-HEV IgG Ab was added to 2 mL of diluted AuNPs
179 (pH 9.2). The solution was stirred gently for 1 h, and 10% BSA solution was added at the ratio
180 1:1 to saturate the surface of the AuNPs for minimizing the nonspecific binding. The solution
181 was stirred for 1 h and then, was centrifuged at 13,500 g for 15 min at 4°C. The suspension of
182 anti-HEV IgG Ab-conjugated AuNPs (Ab-AuNPs) was re-dispersed in 1 × PBS solution
183 (containing 2% BSA) and stored at 4°C.

184 The conjugation of anti-HEV Ab and AuNPs was confirmed by direct ELISA with anti-
185 rabbit IgG HRP antibody. Briefly, 100 µL of Ab-AuNPs was immobilized in the wells of a
186 microtiter plate and incubated at 4°C overnight. As comparison, 2% BSA and AuNPs were
187 used as negative controls. After the immobilization of analytes, the wells were rinsed with 200
188 µL washing buffer twice. Anti-rabbit IgG HRP was diluted in 2% BSA (1:5000) and 100 µL
189 was added to the well, then incubated for 1 h. After rinsing process, 100 µL/well chromogenic
190 solution in acetate buffer was introduced to each well, and a blue color was developed as a
191 confirmation of binding affinity of anti-IgG to anti-HEV Ab-conjugated to AuNPs. After a
192 reaction time of 5–10 min, 100 µL stop solution was added to the well to stop the reaction,
193 immediately the yellow color substituted the previously blue color. Eventually, the developed
194 color was measured using a microplate reader (Infinite 200 M Plex, TECAN) at 450 nm with
195 reference wavelength of 655 nm.

196

197 *2.6 Blocking of Ab-AuNPs and AuNPs@Ag using BSA*

198 BSA (3%) was used to saturate the surface of AuNPs after the bioconjugation of Ab-
199 AuNPs. After the bioconjugation step, Ab-AuNPs were re-dispersed in 1 × PBS solution. Then,
200 the Ab-AuNPs in PBS were blocked by addition of 3% BSA (BSA/Ab-AuNPs), following by

re-dispersed in solution. Afterwards, BSA/Ab-AuNPs and Ab-AuNPs were applied for capture immunoassay. The blank sample was used to show the background signal and 100 ng/mL HEV-LPs was used as the positive sample containing target analytes. BSA/Ab-AuNPs were demonstrated in the capture immunoassay without applying silver deposition solution to highlight the signal amplification concept of the AuNPs@Ag capture immunoassay.

The catalytic activity of the corresponding Ab-AuNPs with and without BSA blocking process and after the silver shell deposition was investigated. After 1 min of reaction, the stop solution was added, and the absorbance was measured at 450 nm/655 nm using a microplate reader (Infinite 200 M Plex, TECAN, Kanagawa, Japan).

2.7 Signal-amplified Colorimetric Detection of HEV-LPs and HEVs

The proposed silver-deposited AuNPs (AuNPs@Ag) immunoassay was applied to HEV-LPs detection. Initially, the platform was prepared by immobilizing 100 µL of capturing anti-HEV IgG Ab with final concentration of 1 µg/mL in PBS solution in the wells of the microtiter plate overnight at 4°C. Afterward, the wells were rinsed twice with washing buffer after each step, except if it is mentioned otherwise. To prevent any unspecific binding to the well matrix, the wells were blocked with 5% BSA in PBS solution for 2 h. Subsequently, series dilution of HEV-LPs in PBS solution was introduced, shaken and incubated for 1 h. Then, 100 µL of Ab-AuNPs was added and further incubated for 1 h. The captured HEV-LPs were bound to the Ab-AuNPs, and the immuno-sandwich structure of Ab/HEV-LPs/Ab-AuNPs was formed.

Prior to the addition of silver deposition solution, the well was rinsed with washing buffer and followed by DI water to remove chloride ions from the system. For signal amplification, 100 µL of silver deposition solution was added to the immuno-sandwich structure, allowing the reduction of silver ions on the surface of the AuNPs. The Ag^{+} ions were attracted by the negatively charged surface of AuNPs and reduced by the given reactant HQ on the surface of

AuNPs. Thus, *in situ* AuNPs@Ag had been formed within 15 min. After four times washing step with DI water, 100 µL chromogen solution was introduced to the well containing the Ab/HEV-LPs/Ab-AuNPs@Ag immuno-sandwich structure. Blue color was developed rapidly. After 1-min reaction time, 100 µL stop solution was added to the well to stop the reaction while an immediate the yellow color substituted the previous blue color. Eventually, the developed color was measured using a microplate reader (Infinite 200 M Plex, TECAN) at 450 nm with reference wavelength of 655 nm.

HEV detection in fecal specimen was also carried out using AuNPs@Ag capture immunoassay, followed by the same procedures in HEV-LPs detection. The samples were collected from 4 to 43 dpi and were diluted 30 times in PBS buffer before evaluation. For capture ELISA, the protocol was the same as the HEV-LPs detection with the sample containing HEV in PBS buffer.

3. Result and Discussion

3.1 Principle of Silver-shell Deposition on Gold-core Nanozyme

The proposed immunoassay is a modified procedure of capture ELISA assay applying the AuNPs@Ag nanozyme, instead of standard HRP to achieve high sensitivity in rapid process. The process of this proposed immunoassay can be divided in three parts which are schematically presented in **Fig. 1** for easy understanding. Initially, the target virus was introduced to the reaction chamber and formed immuno-sandwich structure between immobilized antibodies on the well and Ab-AuNPs via antibody-antigen interaction, following the standard protocol of immunoassay. In **Fig. S1**, the antibodies were assayed to show its binding capability to recognize the HEV-LPs. Unbound Ab-AuNPs were removed by washing process (**Fig. 1A**). Then, the surface of AuNPs were treated with silver solution and formed AuNPs@Ag (**Fig. 1B**) by HQ reduction. Generally, HQ would tend cannot reduce the Ag^{+} ions

due to its low redox potential (–0.3 V) which had to overcome the high negative redox potential of isolated silver (–1.8 V). However, in presence of existing core of AuNPs, having positive redox value of +0.799, it can smoothly reduce the Ag^+ to Ag nanoparticle on the surface of AuNP [38]. To demonstrate this statement in this work, the silver deposition was demonstrated to AuNPs in the format of Signal-to-Noise ratio referencing the blank solution with no AuNPs. Based on the function of time, the silver deposition was occurred increasing to certain maximal deposition, but the silver deposition was not taking place without the presence of AuNPs which could act as the seed of this deposition. (**Fig. S2**). Further, after the maximal incubation time, the signal-to-noise ratio decreased because the increasing thickness of the silver shell which was proportional to the incubation time (as presented in Fig. S2) could affect the immunocomplex formation, lowering the sensitivity in the virus detection.

After that, the unreacted the Ag^+ ions and HQ had been removed and the reaction well had been introduced with chromogen solution, consisting of TMB and H_2O_2. Originally, Au nanozyme played the catalytic effect on the oxidation of TMB, forming visible blue colour, by H_2O_2 (**Fig. 1C**). The oxidation of TMB was enhanced drastically in presence of Ag^+ ions, generating from the decomposition of silver shell of AuNPs@Ag by H_2O_2. As a metal precursor, Ag^+ ions have strong negative reducing potential toward the TMB solution [39]. The colouration indicates the presence of the HEV-LPs whereas the intensity of the colour represents the concentration of HEV-LPs in the solution. By this means, in this study, the colorimetric immunoassay for HEV-LPs has been replaced from catalytic activity of HRP to peroxidase-like activity with AuNPs@Ag nanozyme where the enhanced sensitivity has been achieved due to the decomposition of silver-shell on the surface of AuNPs.

<< Fig. 1>>

3.2 Physiochemical Characterization

According to our hypothesis, the synthesized AuNPs@Ag formation plays the key role for the enhanced sensitivity of the *in situ* virus detection process. To prove the formation of the AuNPs@Ag core shell structure, initially, the system was characterised without addition of any virus. AuNPs were synthesized by reducing gold ions by trisodium citrate. Trisodium citrate acts as reductant and coating agent for synthesized AuNPs. The reddish colour AuNPs was characterized by UV-Vis spectrophotometry, showing the surface resonance peak at 508 nm (**Fig. S3**) [40]. As shown in the TEM image of **Fig. 2A**, the dark spherical structure indicates the homogeneous distribution of AuNPs with the size of around 14 nm. To confirm the silver deposition process, the silver solution with HQ were applied to the as synthesized AuNPs. In **Fig. 2B**, the high resolution (HR)-TEM image shows around 26 nm-size nanoparticles with two-different layers; darker side on the inside as the Au core and brighter side surrounding it due to the less dense electron shell of Ag compared to Au. The AuNP size was not changed significantly inside the core, showing the silver deposition occurred mainly on the surface of AuNPs with the shell thickness around 6 to 7 nm. The hydrodynamic size of AuNPs were found 13.66 ± 3.66 nm with polydispersity index of 0.273 which increased to 24.4 nm after the Ag deposition, measured by DLS (**Fig. 2C**) which is perfectly corroborated with their TEM calculation. The negatively charged of AuNPs was showed the zeta potential of –30 mV which decreased to –15 mV after the silver shell was deposited (**Fig. 2D**). From the above results, it can be concluded that the AuNPs were successfully coated with Ag to form the core-shell in presence of the Ag^+ ions and HQ. The aim of this present work is to apply this finding for the *in situ* detection of HEV in fecal sample.

<< Fig. 2>>

3.3 Bioconjugation of Anti-HEV IgG Ab to AuNPs

The anti-HEV IgG antibody and AuNPs were bound via physical adsorption which was confirmed by the anti-IgG rabbit ELISA technique. Compared to bare AuNPs, Ab-AuNPs showed obvious higher absorbance in ELISA which indicates the successful binding of antibodies on the AuNPs (**Fig. S4**). The binding was also confirmed by the UV-Visible plasmonic peak shift of AuNPs (**Fig. S3**) due to the adsorption of the protein on the surface of AuNPs. The 6 nm shift was observed from 512 nm to 518 nm without any significant change in intensity throughout the absorbance spectrum. The small decrease of intensity was noticed due to some loss of AuNPs in the centrifugation process. The physical adsorption method in antibody and nanoparticles has been favourable in term of simplicity due to spontaneous and readily adsorption of protein on the surface of AuNPs [41, 42].

3.4 Role of BSA as Blocking Agent

The blocking process by BSA is an important step to saturate the surface of AuNPs which can prevent the non-specific binding with AuNPs and hence lowering the detection limit. As shown in **Fig. 3**, the Ab-AuNPs@Ag showed much higher background signal compared to its BSA-blocked condition (BSA/Ab-AuNPs@Ag). Without silver deposition (BSA/Ab-AuNPs), the signal was as low as the control, showing insufficient signal generator for the detection of HEV-LPs. In case of silver enhanced condition, the observed signal in the presence of HEV-LPs showed higher intensity by BSA/Ab-AuNPs@Ag compared to Ab-AuNPs@Ag. It means that the BSA blocking not only reduce the background noise but also enhance the generating signal of the immunoassay. This may be due to the fact that the antibody of the BSA/Ab-AuNPs@Ag can only bind to the captured HEV-LPs without any non-specific binding in the well due to the covered surface of BSA. Therefore, during the washing step, the possibility of losing immuno-sandwich structure, attached by the non-specific interaction, becomes

ignorable. Similar observation of lower background signal in the BSA blocking on AuNPs compared to non-BSA blocking was also noticed in case of fecal HEV also as shown in **Fig. S5**. Besides the BSA blocking effect, it was necessary to highlight the occurrence of the signal amplification by the silver deposition in the fecal matrix. Without the addition of the silver deposition, only AuNPs-based immunoassay can generate low detection signal to the HEV, however, after the addition of silver deposition, the increasement signal was noticeable. The above observation showed that the amplification technique using the silver deposition could be applied in matrix complex condition but there is a need to saturate the surface of AuNPs with BSA to generate consistent signal with lower background noise which can significantly enhance the detection limit of the proposed sensor.

<< Fig. 3>>

3.5 HEV-LPs Detection using Proposed Immunoassay

Detection of HEV by AuNPs@Ag capture immunoassay is the final goal of this current work. To confirm its applicability, we have carried out the analysis in step by step optimization process. To confirm the specificity, the proposed immunoassay was first applied with 10 ng/mL of different viruses of influenza virus A, NoV, zika virus and BSA as a negative control along with the target HEV-LPs (**Fig. 4**). Intense colour change was observed in case of HEV-LPs whereas all other viruses did not show any significant coloration as expected (inset of **Fig. 4**). As the specificity of this proposed immunoassay is solely dependent on the antigen-antibody interaction, it is quite expected to get the desired selectivity. Therefore, the intensity of the HEV-LP was found almost 6-fold higher compared to all others, confirming that any other part of the immunoassays is not taking part for any non-specific interaction with the viruses.

<< Fig. 4>>

As the platform was already verified to generate selective signal towards HEV-LPs, a series of diluted HEV-LPs solution was assayed with the proposed immunoassay. The absorbance of the developed from the TMB catalytic oxidation was measured and plotted in log scale to show better linearity fit to the change of the HEV-LPs concentration. Based on the increasing concentration of HEV-LPs in the sample, the gradual enhancement of intensity of the immunoassays with its colour was developed. The generated signal was compared to indirect conventional ELISA using HRP-conjugated to anti-IgG/anti-HEV immunoassay. As shown in the **Fig. 5**, in HRP-based ELISA, HEV-LPs lower than 27 pg/mL could not be detected whereas, in the present work, the AuNPs@Ag capture immunoassay could generate distinct detection signal with dynamic range from the lowest concentration used of 10 pg/mL to 10 ng/mL HEV-LPs with correlation coefficient of 0.988. The LOD was calculated around 4.32 pg/mL based on the slope of the calibration line, the intercept of the linear function and the 3.3 times of the SD_{blank} of the blank (control) [20]. In addition, the stability of this immunoassay was tested up to 4 weeks. Up to second week, the detection signal was relatively around 98%. At the third week, the signal detection decreased around 20%, showing the relative activity up to 70% in fourth week. This indicated the proposed immunoassay could be optimally used for up to two weeks (**Fig. S6**). Major factor could attribute to the stability of the antibody and the conjugation of the Ab-AuNPs.

<< Fig. 5>>

3.6 Detection of HEV by AuNPs@Ag Capture Immunoassay.

To screen performances of our proposed method, we have provided the comparative performances with the standard indirect ELISA where proposed sensor shows satisfactory good performance in term of sensitivity and detection range. However, the real challenge has been

arisen in case of fecal samples where matrix has severe interfering reagents. In that case, the gold standard in determining any viral infection is based on the RNA measurement by RT-PCR. To evaluate the applicability in patients or animals' sample, the developed immunoassay was further applied for the detection of HEV in fecal specimens from a G7 HEV-infected monkey. In **Fig. 6**, RNA copy numbers measured by RT-qPCR were double-blindly compared with the obtained data from this proposed immunoassay. The signal from the proposed immunoassay was measured in change of absorbance (ΔAbs) with the preference to the blank sample (PBS). The infection peak was shown within first week to second week and then gradually decreased to undetectable amount.

According to the RT-qPCR, the positive results were observed up to 18 dpi whereas the later values were undetectable which consider negative. Based on the infection cycle of HEV and the result on the RT-qPCR, the undetectable HEV RNAs (open blue square) demonstrated that the monkey did not carry HEV in that state (non-infected monkey). Those fecal specimens were determined as the negative controls in the monitoring assay. On the basis on those negative samples and the blank signal, the cut-off value was determined for our proposed immunoassay (mean of the blank × 2) and the cut-off line was designated at 0.1 ΔAbs for this work. As depicted in the **Fig. 6**, the trend of the obtained result from the AuNPs@Ag capture immunoassay was similar with the RT-qPCR results in quite satisfactory manner, confirming the applicability of this method for real samples. However, in **Fig. S7**, the linear correlation of the signal generated from the proposed immunoassay was not satisfactory with R^2 of 0.952, although the residual plot showed randomize distribution (**Fig. S7**). This could occur due to different biomolecules as the target, in which the proposed immunoassay and RT-qPCR targeted and quantified proteins and RNA respectively or due to the matrix effect in the performance. Nevertheless, the signal correlation plot showed linear trend despite its low coefficient.

Compared to the recent progress of the virus biosensor (**Table 1**), although the sensitivity of this method was lower than the electrochemical sensor, this naked-eye monitoring purpose capture immunoassay had higher sensitivity to the fluorometric system up to picogram level detection with simple protocol and easy determination of presence of virus. This can highlight the advantage of this AuNPs@Ag capture immunoassay in biological sample, showing an enhanced nanozyme-based immunoassay for direct detection of HEV.

<< Fig. 6>>

4. Conclusion

The proposed immunoassay utilizing Ag deposition on AuNPs enhanced the peroxidase-like activity significantly as a nanozyme. Silver deposition on the gold showed a significantly amplified signal in the detection of HEV-LPs and HEV compared to conventional HRP-based ELISA as well as the bare AuNP based immunoassays. This proposed immunoassay showed highly sensitive and selective toward the HEV compared to various viral agents even can be observable in naked eyes. The performed assay for HEV-LPs in buffer was found to be able to detect as low as 10 pg/mL in a linear concentration range of 10 pg/mL to 10 ng/mL. It was also successfully applied for the detection of fecal samples from HEV-infected monkey over a period of 45 days of infection and found comparable with the data obtained from RT-qPCR. As the AuNPs@Ag capture immunoassay showed improved sensitivity towards specific infectious disease agent, we hope that this proposed method can be served as an excellent monitoring system for virus detection.

Ethical Approval

The experiments were reviewed by the National Institute of Infectious Diseases (NIID) Ethics Committee and carried out according to the "Guides for Animal Experiments Performed at NIID" under code 514014.

Conflict of interests

The authors declare no competing financial interests.

Acknowledgements

This work was supported and partly by the Bilateral Joint Research Project of the JSPS, Japan. We thank Professor Kouichi Morita of the Institute of Tropical Medicine, Nagasaki University, and Dr. Fuyuki Abe from Shizuoka Institute of Environment and Hygiene, for kindly providing the Zika virus and clinically isolated norovirus. ADC sincerely thank the Japan Society for the Promotion of Science (JSPS) for a postdoctoral fellowship (No. P17359). This research was partially supported by the Japan Agency for Medical Research and Development (AMED) under grant nos. JP19fk0210053, JP19fk0210043, and JP19fk0108102.

Appendix A. Supplementary data

Absorbance of AuNPs and Ab-AuNPs, ELISA for bioconjugation confirmation of anti-HEV Ab/AuNPs, influence of BSA-blocking on AuNPs@Ag in capture immunoassay, ELISA for recognition of anti-HEV-Ab, comparison of HEV detection. Supplementary material related to this article can be found, in the online version, at doi:https://doi:

References

[1] K. Himmelsbach, D. Bender, E. Hildt, Life cycle and morphogenesis of the hepatitis E virus, Emerging microbes & infections, 7 (2018) 196.

[2] U. Navaneethan, M. Al Mohajer, M.T. Shata, Hepatitis E and pregnancy: understanding the pathogenesis, Liver international, 28 (2008) 1190–1199.

[3] S.K. Acharya, Hepatitis E and acute liver failure in pregnancy, J. Clin. Exp. Hepatol., 3 (2013) 213–224.

[4] J.G. Melgaço, N.R. Gardinali, V.d.M.d. Mello, M. Leal, L.L. Lewis-Ximenez, M.A. Pinto, Hepatitis e: Update on prevention and control, BioMed research international, 2018 (2018).

[5] S. Zhang, D. Tian, Z. Zhang, J. Xiong, Q. Yuan, S. Ge, J. Zhang, N. Xia, Clinical significance of anti-HEV IgA in diagnosis of acute genotype 4 hepatitis E virus infection negative for anti-HEV IgM, Dig. Dis. Sci., 54 (2009) 2512.

[6] Y.-J. Chen, M. Chen, Y.-C. Hsieh, Y.-C. Su, C.-H. Wang, C.-M. Cheng, A.-P. Kao, K.-H. Wang, J.-J. Cheng, K.-H. Chuang, Development of a highly sensitive enzyme-linked immunosorbent assay (ELISA) through use of poly-protein G-expressing cell-based microplates, Sci. Rep., 8 (2018).

[7] E. Stern, A. Vacic, C. Li, F.N. Ishikawa, C. Zhou, M.A. Reed, T.M. Fahmy, A nanoelectronic enzyme‐linked immunosorbent assay for detection of proteins in physiological solutions, small, 6 (2010) 232–238.

[8] D. Ramana, A. Capoor, R. Sashidhar, R.V. Bhat, Limitations in the use of horseradish peroxidase as an enyzme probe in the development of a homogeneous immunoassay for aflatoxin B 1, Fresenius J. Anal. Chem., 352 (1995) 43–48.

[9] S.R. Ahmed, J. Kim, T. Suzuki, S. Neethirajan, J. Lee, E.Y. Park, In situ self-assembly of gold nanoparticles on hydrophilic and hydrophobic substrates for influenza virus-sensing platform, Sci. Rep., 7 (2017) 44495.

[10] L. Gao, J. Zhuang, L. Nie, J. Zhang, Y. Zhang, N. Gu, T. Wang, J. Feng, D. Yang, S. Perrett, Intrinsic peroxidase-like activity of ferromagnetic nanoparticles, Nature Nanotechnol., 2 (2007) 577.

[11] Q. Wang, H. Wei, Z. Zhang, E. Wang, S. Dong, Nanozyme: An emerging alternative to natural enzyme for biosensing and immunoassay, TrAC, Trends Anal. Chem., 105 (2018) 218–224.

[12] L. Qin, X. Wang, Y. Liu, H. Wei, 2D-Metal–Organic-Framework-Nanozyme Sensor Arrays for Probing Phosphates and Their Enzymatic Hydrolysis, Anal. Chem., 90 (2018) 9983–9989.

[13] L. Wu, W. Yin, K. Tang, D. Li, K. Shao, Y. Zuo, J. Ma, J. Liu, H. Han, Enzymatic biosensor of horseradish peroxidase immobilized on Au-Pt nanotube/Au-graphene for the simultaneous determination of antioxidants, Anal. Chim. Acta, 933 (2016) 89–96.

[14] Y. Huang, J. Ren, X. Qu, Nanozymes: classification, catalytic mechanisms, activity regulation, and applications, Chem. Rev., 119 (2019) 4357–4412.

[15] S. Wang, W. Chen, A.L. Liu, L. Hong, H.H. Deng, X.H. Lin, Comparison of the peroxidase‐like activity of unmodified, amino‐modified, and citrate‐capped gold nanoparticles, Chemphyschem, 13 (2012) 1199–1204.

[16] M.N. Karim, S.R. Anderson, S. Singh, R. Ramanathan, V. Bansal, Nanostructured silver fabric as a free-standing NanoZyme for colorimetric detection of glucose in urine, Biosens. Bioelectron., 110 (2018) 8–15.

[17] Y. Fu, X. Zhao, J. Zhang, W. Li, DNA-based platinum nanozymes for peroxidase mimetics, J. Phys. Chem. C, 118 (2014) 18116–18125.

[18] H. Wei, E. Wang, Nanomaterials with enzyme-like characteristics (nanozymes): next-generation artificial enzymes, Chem. Soc. Rev., 42 (2013) 6060–6093.

[19] S. Oh, J. Kim, V.T. Tran, D.K. Lee, S.R. Ahmed, J.C. Hong, J. Lee, E.Y. Park, J. Lee, Magnetic nanozyme-linked immunosorbent assay for ultrasensitive influenza A virus detection, ACS Appl. Mater. Interfaces, 10 (2018) 12534–12543.

[20] I.M. Khoris, K. Takemura, J. Lee, T. Hara, F. Abe, T. Suzuki, E.Y. Park, Enhanced colorimetric detection of norovirus using in-situ growth of Ag shell on Au NPs, Biosens. Bioelectron., 126 (2019) 425–432.

[21] X. Wang, L. Qin, M. Zhou, Z. Lou, H. Wei, Nanozyme sensor arrays for detecting versatile analytes from small molecules to proteins and cells, Anal. Chem., 90 (2018) 11696–11702.

[22] Y. Tao, Y. Lin, Z. Huang, J. Ren, X. Qu, Incorporating Graphene Oxide and Gold Nanoclusters: A Synergistic Catalyst with Surprisingly High Peroxidase‐Like Activity Over a Broad pH Range and its Application for Cancer Cell Detection, Adv. Mater., 25 (2013) 2594–2599.

[23] P. Pachfule, S. Kandambeth, D.D. Díaz, R. Banerjee, Highly stable covalent organic framework–Au nanoparticles hybrids for enhanced activity for nitrophenol reduction, Chem. Commun., 50 (2014) 3169–3172.

[24] N. Cheng, Y. Song, M.M. Zeinhom, Y.-C. Chang, L. Sheng, H. Li, D. Du, L. Li, M.-J. Zhu, Y. Luo, Nanozyme-mediated dual immunoassay integrated with smartphone for use in simultaneous detection of pathogens, ACS Appl. Mater. Interfaces, 9 (2017) 40671–40680.

[25] L. Russo, J. Leva Bueno, J.F. Bergua, M. Costantini, M. Giannetto, V. Puntes, A. de la Escosura-Muñiz, A. Merkoçi, Low-Cost Strategy for the Development of a Rapid Electrochemical Assay for Bacteria Detection Based on AuAg Nanoshells, ACS Omega, 3 (2018) 18849–18856.

[26] P.-C. Kuo, C.-W. Lien, J.-Y. Mao, B. Unnikrishnan, H.-T. Chang, H.-J. Lin, C.-C. Huang, Detection of urinary spermine by using silver-gold/silver chloride nanozymes, Anal. Chim. Acta, 1009 (2018) 89–97.

[27] A. Dutta Chowdhury, N. Agnihotri, R.-a. Doong, A. De, Label-free and nondestructive separation technique for isolation of targeted DNA from DNA–protein mixture using magnetic Au–Fe3O4 nanoprobes, Anal. Chem., 89 (2017) 12244–12251.

[28] S. Barman, M. Hossain, H. Yoon, J.Y. Park, Trimetallic Pd@ Au@ Pt nanocomposites platform on-COOH terminated reduced graphene oxide for highly sensitive CEA and PSA biomarkers detection, Biosens. Bioelectron., 100 (2018) 16–22.

[29] S.W. Kang, Y.W. Lee, Y. Park, B.-S. Choi, J.W. Hong, K.-H. Park, S.W. Han, One-pot synthesis of trimetallic Au@ PdPt core–shell nanoparticles with high catalytic performance, ACS Nano, 7 (2013) 7945–7955.

[30] H. Wang, K. Wan, X. Shi, Recent advances in nanozyme research, Adv. Mater., (2018) 1805368.

[31] Y. Zhou, B. Liu, R. Yang, J. Liu, Filling in the gaps between nanozymes and enzymes: challenges and opportunities, Bioconjugate Chem., 28 (2017) 2903–2909.

[32] L. Tang, J. Casas, M. Venkataramasubramani, Magnetic nanoparticle mediated enhancement of localized surface plasmon resonance for ultrasensitive bioanalytical assay in human blood plasma, Anal. Chem., 85 (2013) 1431–1439.

[33] S. Xu, X. Ji, W. Xu, X. Li, L. Wang, Y. Bai, B. Zhao, Y. Ozaki, Immunoassay using probe-labelling immunogold nanoparticles with silver staining enhancement via surface-enhanced Raman scattering, Analyst, 129 (2004) 63–68.

[34] R. Liu, X. Liu, Y. Tang, L. Wu, X. Hou, Y. Lv, Highly sensitive immunoassay based on immunogold− silver amplification and inductively coupled plasma mass spectrometric detection, Anal. Chem., 83 (2011) 2330–2336.

[35] S. Gupta, S. Huda, P.K. Kilpatrick, O.D. Velev, Characterization and optimization of gold nanoparticle-based silver-enhanced immunoassays, Anal. Chem., 79 (2007) 3810–3820.

[36] T.-C. Li, K. Yoshimatsu, S.P. Yasuda, J. Arikawa, T. Koma, M. Kataoka, Y. Ami, Y. Suzaki, L.T.Q. Mai, N.T. Hoa, Characterization of self-assembled virus-like particles of rat hepatitis E virus generated by recombinant baculoviruses, J. Gen. Virol., 92 (2011) 2830.

[37] T.-C. Li, Y. Yamakawa, K. Suzuki, M. Tatsumi, M. Razak, T. Uchida, N. Takeda, T. Miyamura, Expression and self-assembly of empty virus-like particles of hepatitis E virus, J. Virol., 71 (1997) 7207–7213.

[38] S.T. Gentry, S.J. Fredericks, R. Krchnavek, Controlled particle growth of silver sols through the use of hydroquinone as a selective reducing agent, Langmuir, 25 (2009) 2613–2621.

[39] R. González-Fuenzalida, Y. Moliner-Martínez, M. González-Béjar, C. Molins-Legua, J. Verdú-Andres, J. Pérez-Prieto, P. Campins-Falco, In situ colorimetric quantification of silver cations in the presence of silver nanoparticles, Anal. Chem., 85 (2013) 10013–10016.

[40] A. Dutta Chowdhury, A.B. Ganganboina, F. Nasrin, K. Takemura, R.-a. Doong, D.I.S. Utomo, J. Lee, I.M. Khoris, E.Y. Park, Femtomolar Detection of Dengue Virus DNA with Serotype Identification Ability, Anal. Chem., 90 (2018) 12464–12474.

560 [41] S. Zhang, Y. Moustafa, Q. Huo, Different interaction modes of biomolecules with citrate-
561 capped gold nanoparticles, ACS Appl. Mater. Interfaces, 6 (2014) 21184–21192.

562 [42] M.H. Jazayeri, H. Amani, A.A. Pourfatollah, H. Pazoki-Toroudi, B. Sedighimoghaddam,
563 Various methods of gold nanoparticles (GNPs) conjugation to antibodies, Sens. Biosens. Res.,
564 9 (2016) 17–22.

565 [43] K. Takemura, O. Adegoke, N. Takahashi, T. Kato, T.-C. Li, N. Kitamoto, T. Tanaka, T.
566 Suzuki, E.Y. Park, Versatility of a localized surface plasmon resonance-based gold
567 nanoparticle-alloyed quantum dot nanobiosensor for immunofluorescence detection of viruses,
568 Biosens. Bioelectron., 89 (2017) 998-1005.

569 [44] Q. Zeng, Y. Zhang, X. Liu, L. Tu, X. Kong, H. Zhang, Multiple homogeneous
570 immunoassays based on a quantum dots–gold nanorods FRET nanoplatform, Chem. Commun.,
571 48 (2012) 1781-1783.

572 [45] X. Wang, Y. Li, H. Wang, Q. Fu, J. Peng, Y. Wang, J. Du, Y. Zhou, L. Zhan, Gold
573 nanorod-based localized surface plasmon resonance biosensor for sensitive detection of
574 hepatitis B virus in buffer, blood serum and plasma, Biosens. Bioelectron., 26 (2010) 404-410.

575 [46] S. Oh, J. Kim, V.T. Tran, D.K. Lee, S.R. Ahmed, J.C. Hong, J. Lee, E.Y. Park, J. Lee,
576 Magnetic nanozyme-linked immunosorbent assay for ultrasensitive influenza A virus detection,
577 ACS Appl. Mater. Interfaces, 10 (2018) 12534-12543.

578 [47] E.M. Linares, C.S. Pannuti, L.T. Kubota, S. Thalhammer, Immunospot assay based on
579 fluorescent nanoparticles for Dengue fever detection, Biosens. Bioelectron., 41 (2013) 180-
580 185.

581 [48] Y. Geng, C. Zhao, W. Huang, T.J. Harrison, H. Zhang, K. Geng, Y. Wang, Detection and
582 assessment of infectivity of hepatitis E virus in urine, J. Hepatol., 64 (2016) 37-43.

583 [49] S. Martin-Latil, C. Hennechart-Collette, L. Guillier, S. Perelle, Method for HEV detection
584 in raw pig liver products and its implementation for naturally contaminated food, Int. J. Food
585 Microbiol., 176 (2014) 1-8.

586 [50] N. Jothikumar, T.L. Cromeans, B.H. Robertson, X. Meng, V.R. Hill, A broadly reactive
587 one-step real-time RT-PCR assay for rapid and sensitive detection of hepatitis E virus, J. Virol.
588 Methods, 131 (2006) 65-71.

589 [51] A.D. Chowdhury, K. Takemura, T.-C. Li, T. Suzuki, E.Y. Park, Electrical pulse-induced
590 electrochemical biosensor for hepatitis E virus detection, Nature communications, 10 (2019).

591

Legend for figures

Fig. 1. Schematic principle of the silver deposited-gold (AuNPs@Ag) nanozyme-based capture immunoassay. (A) Binding of Ab-AuNPs on the captured HEV-LPs, (B) Ag-shell deposition on the surface of AuNPs and (C) Colour development by the catalytic oxidation of TMB by Ag^{+} and H_2O_2.

Fig. 2. Physiochemical properties of AuNPs. (A) TEM image of AuNPs, (B) HR-TEM image of AuNPs@Ag, (C) Hydrodynamic size distribution and (D) Zeta potential of AuNPs (black) and AuNPs@Ag (green).

Fig. 3. Influence of BSA (blocking agents) on the surface of AuNPs in the capture immunoassay with silver deposition solution (error bars represent the standard deviation of triple measurements).

Fig. 4. Specificity test of AuNPs@Ag capture immunoassay for the detection of HEV-LPs compared with 2% BSA, Zika virus (ZV), Influenza virus (IV) and norovirus (NoV). The concentration of HEV-LPs was 10 ng/mL and 1.3 μg/mL for IV, 10^7 copies/mL for NoV, and 10^7 RNA copies/mL for ZV. The inset image showed the colour formation of the immunoassays after virus addition. (error bars represent the standard deviation of triple measurements).

Fig. 5. Concentration-dependent detection of HEV-LPs using AuNPs@Ag capture immunoassay. HRP-based indirect ELISA was also carried out to compare the performance of this proposed immunoassay. Error bars represent the relative standard deviation of triple measurements. ΔAbs was defined as the change of absorbance to the blank.

Fig. 6. Comparison of the HEV detection sensitivity between the proposed AuNPs@Ag capture immunoassay (close circles) and RT-qPCR (closed squares) in fecal specimens (error bars represents the standard deviation of triple measurements). Open squares represent the viral RNAs which are undetectable in RT-qPCR.

618 **Table 1.**

619 Comparison of recent virus detection

Target Virus	Linear range	Detection limit	References
Influenza virus (Fluorometric)	$1–10 \times 10^{-11}$ g mL^{-1}	3×10^{-10} g mL^{-1}	[43]
HBV (Fluorometric)	$>264 \times 10^{-9}$ g mL^{-1}	8.3×10^{-9} g mL^{-1}	[44]
HBV (Fluorometric)	0.01–1 IU mL^{-1}	0.4 IU mL^{-1}	[45]
Influenza A virus (Colorimetric)	$5 \times 10^{-15} – 5 \times 10^{-6}$ g mL^{-1}	44.2×10^{-15} g mL^{-1}	[46]
Dengue RNA (Fluorometric)	$5–500 \times 10^{-9}$ g mL^{-1}	5.2×10^{-9} g mL^{-1}	[47]
HEV RNA (RT-qPCR)	$10^3–10^6$ IU mL^{-1}	2.1×10^4 IU mL^{-1}	[48]
HEV RNA (RT-qPCR)	8.75×10^3– 8.75×10^4 copies mL^{-1}	8.75×10^3 copies mL^{-1}	[49]
HEV RNA (RT-qPCR)	$10–10^9$ copies mL^{-1}	10 copies mL^{-1}	[50]
HEV-LP (Electrochemical)	$10^{-12}–10^{-15}$ g mL^{-1}	8×10^{-14} g mL^{-1}	[51]
HEV-LPs	$8.75 \times 10^{-8}– 10^{-11}$ g mL^{-1}	4.3×10^{-12} g mL^{-1}	This work

620

Fig. 1, Khoris et al.

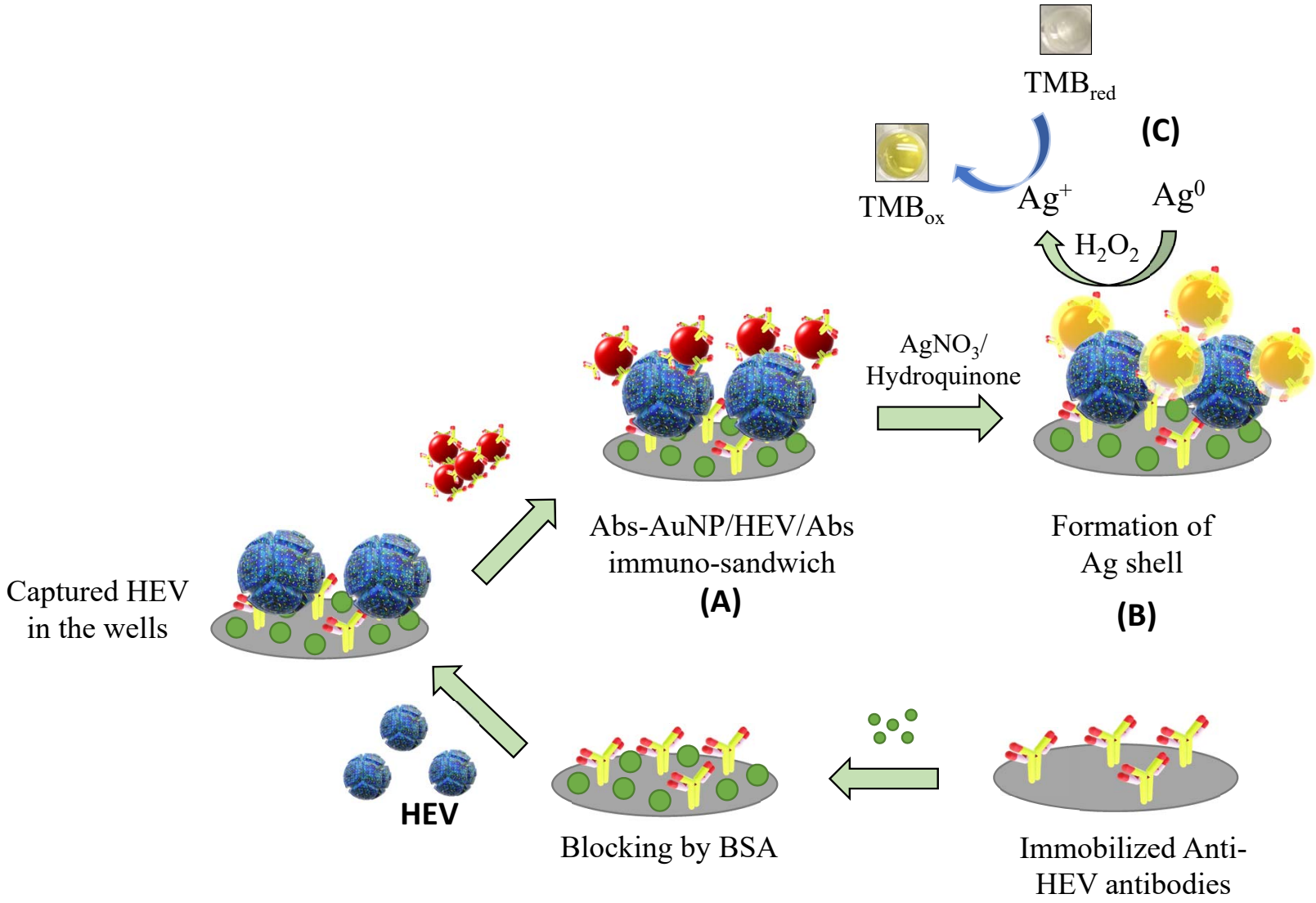

Fig. 2, Khoris et al.

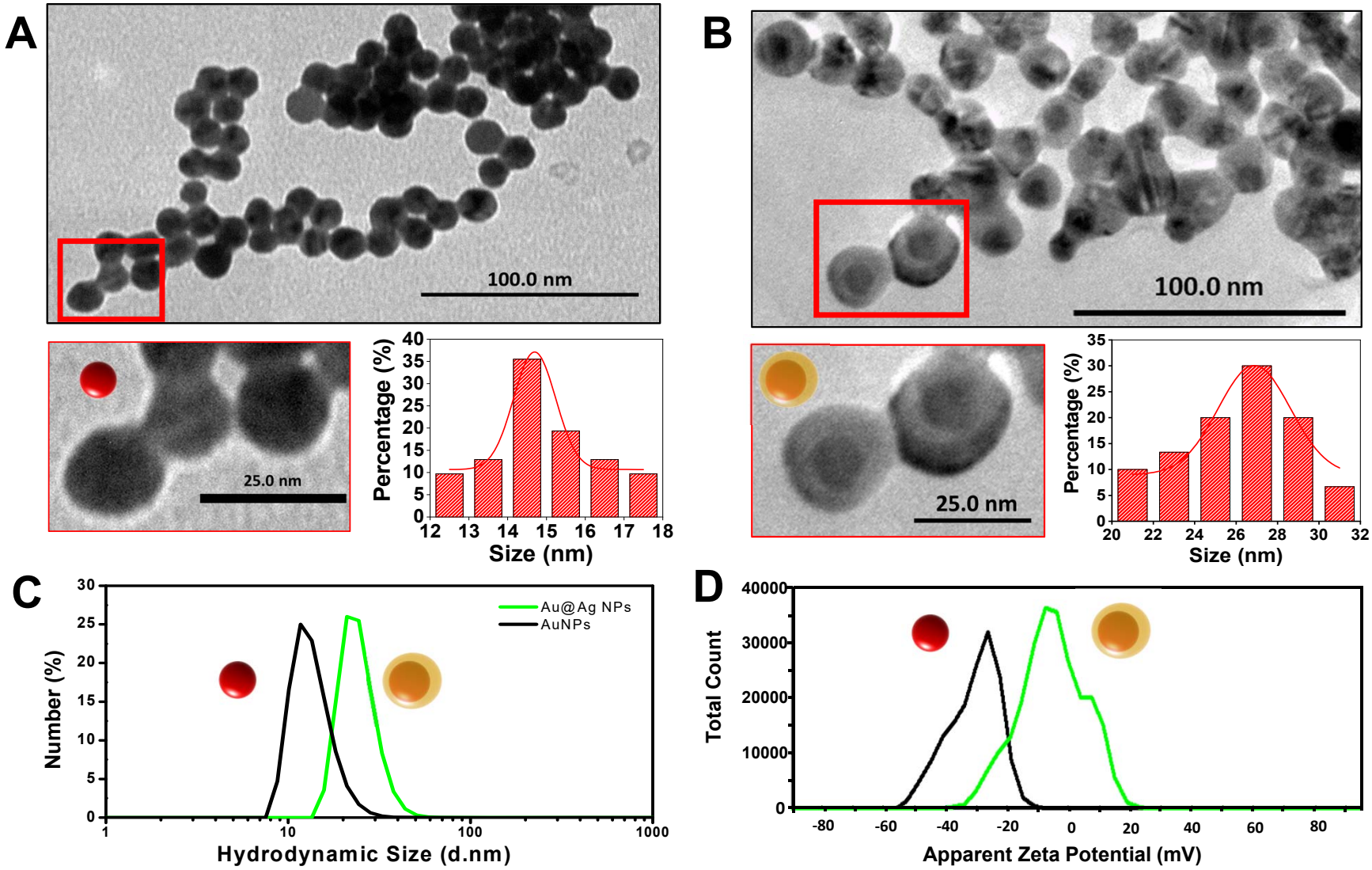

Fig. 3, Khoris et al.

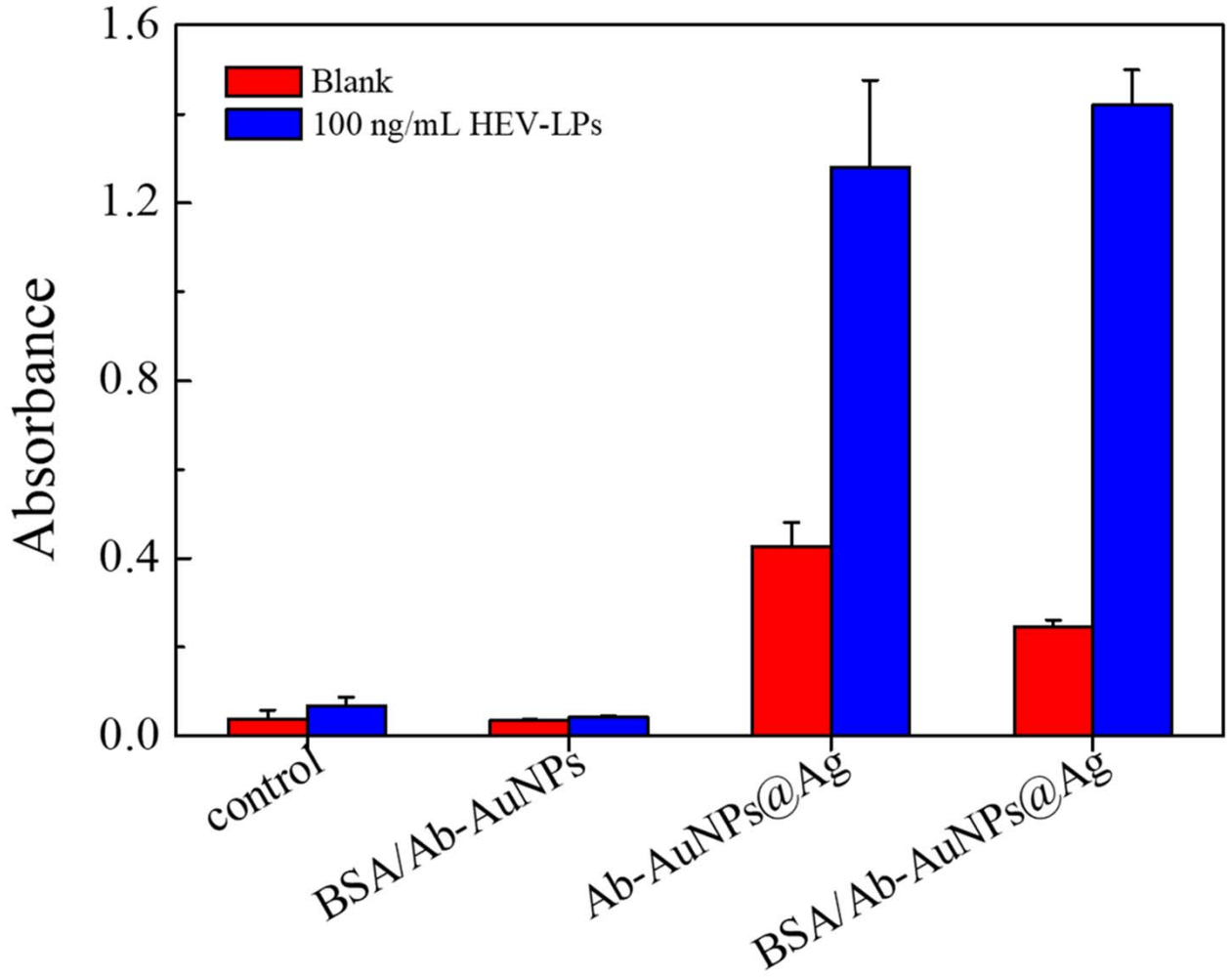

Fig. 4, Khoris et al.

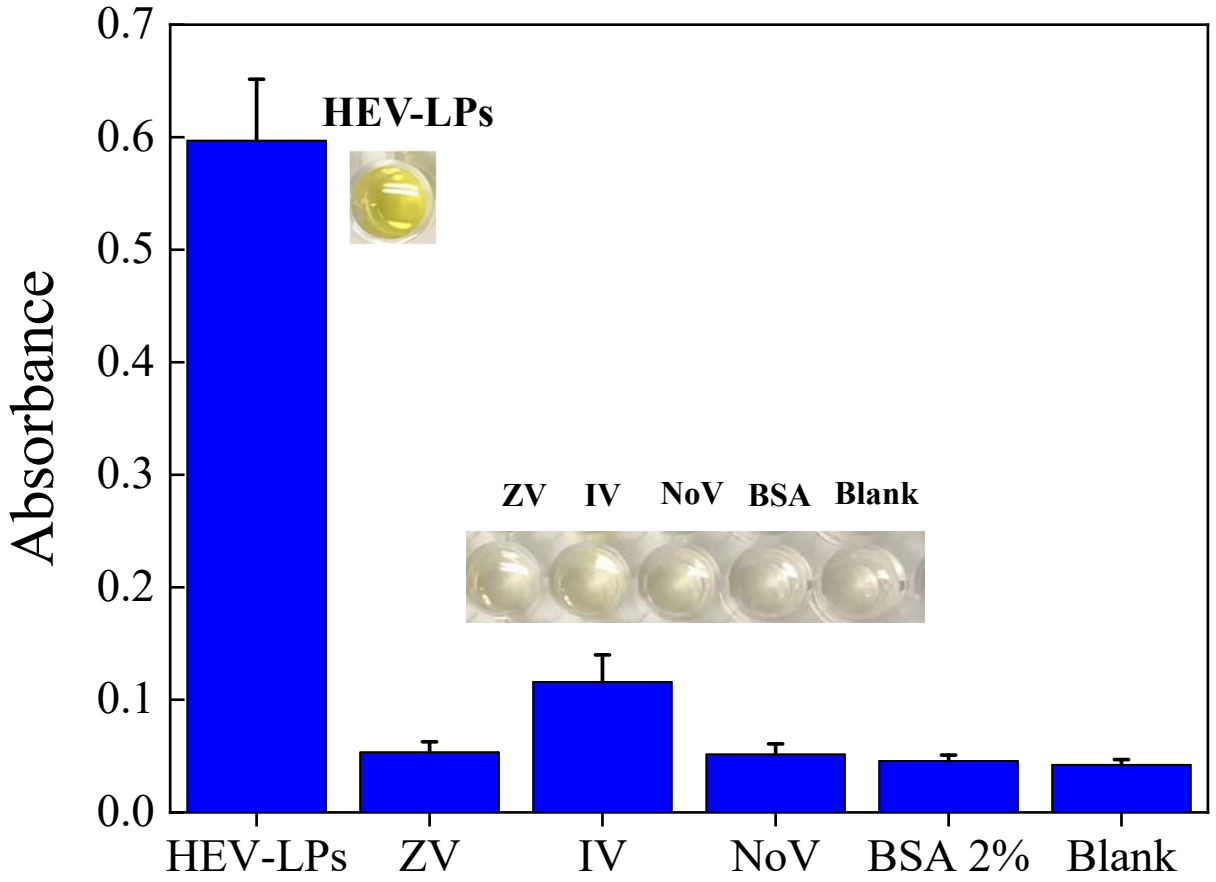

Fig. 5, Khoris et al.

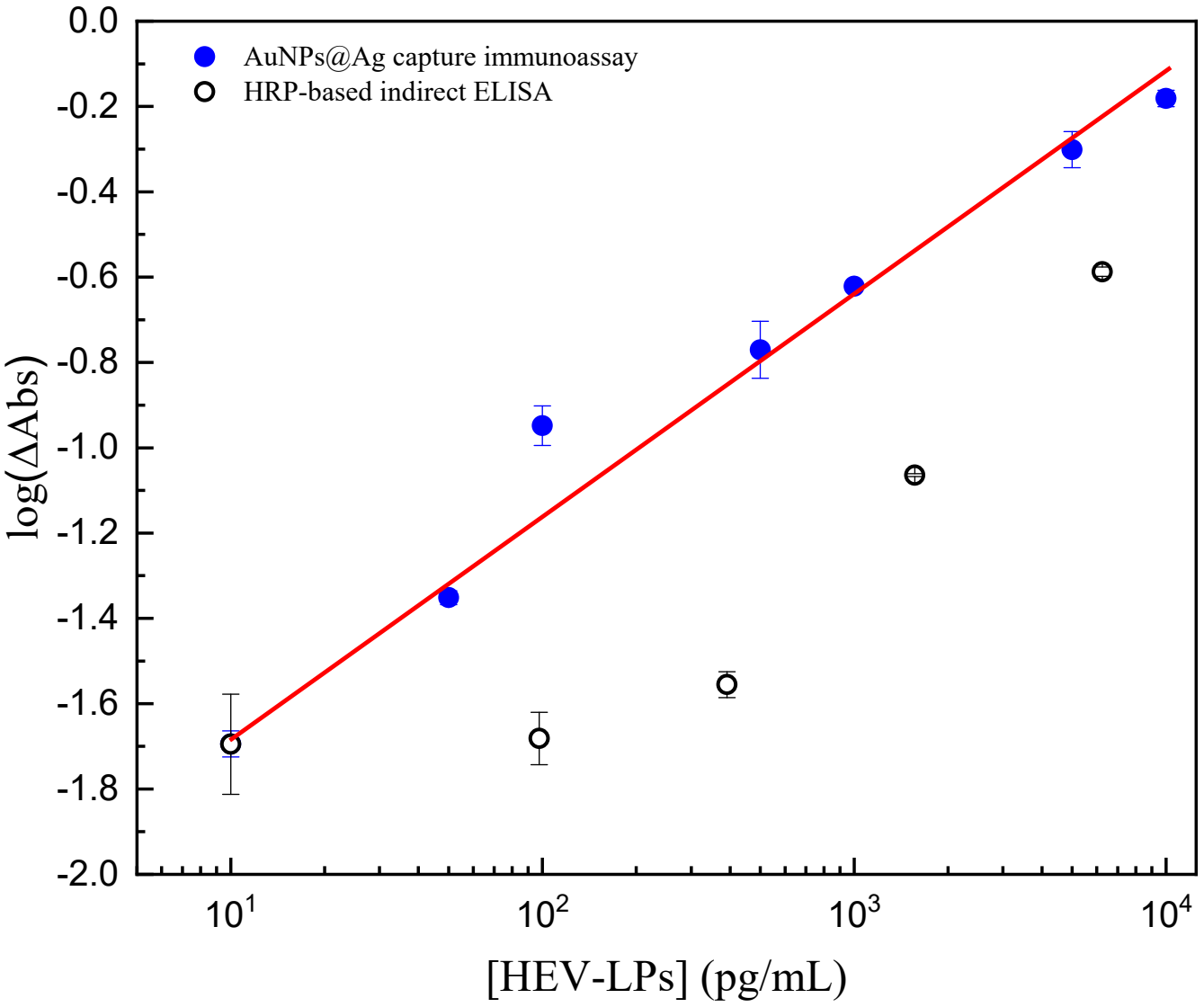

Fig. 6, Khoris et al.

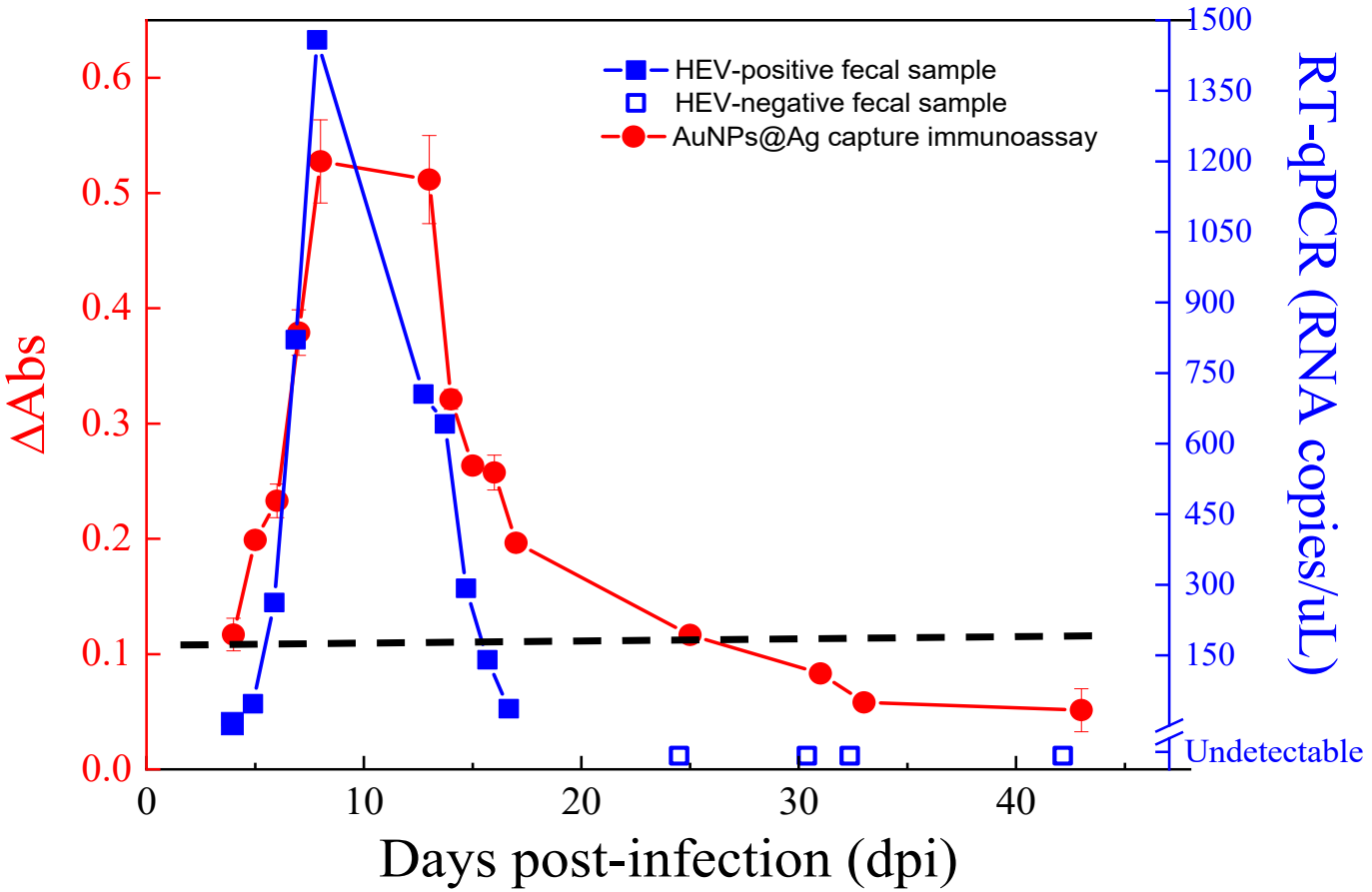

Supplementary material

Advancement of capture immunoassay for real-time monitoring of hepatitis E virus-infected monkey

Indra Memdi Khoris[a], Ankan Dutta Chowdhury[b], Tian-Cheng Li[c], Tetsuro Suzuki[d], Enoch Y. Park[a,b,*]

[a] *Department of Applied Biological Chemistry, College of Agriculture, Graduate School of Integrated Science and Technology, Shizuoka University, 836 Ohya Suruga-ku, Shizuoka 422-8529, Japan*

[b] *Research Institute of Green Science and Technology, Shizuoka University, 836 Ohya Suruga-ku, Shizuoka 422-8529, Japan*

[c] *Department of Virology 2, National Institute of Infectious Diseases, 4-7-1 Gakuen, Musashimurayam-shi, Tokyo 208-0011, Japan*

[d] *Department of Infectious Disease, Hamamatsu University School of Medicine, Handayama, Hamamatsu 431-3125, Japan*

E-mail:

indra.memdi.khoris.17@shizuoka.ac.jp (IMK)
ankan.dutta.chowdhury@shizuoka.ac.jp (ADC)
litc@nih.go.jp (TCL)
tesuzuki@hama-med.ac.jp (TS)
park.enoch@shizuoka.ac.jp (EYP)

[*]Corresponding author: Research Institute of Green Science and Technology, Shizuoka University, 836 Ohya Suruga-ku, Shizuoka 422-8529, Japan.
E-mail address: park.enoch@shizuokac.jp

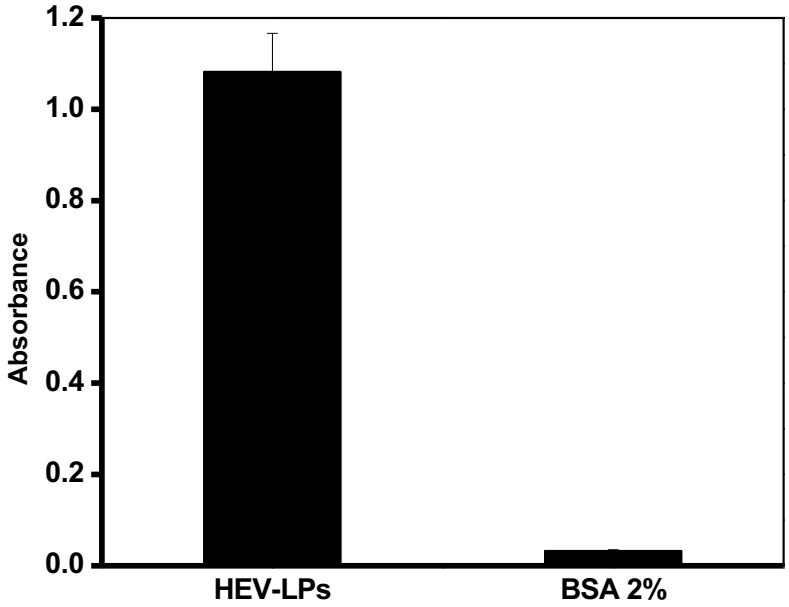

Fig. S1. ELISA for recognition of anti-HEV Ab to HEV-LPs. The error bars represent the standard deviation of triple measurements.

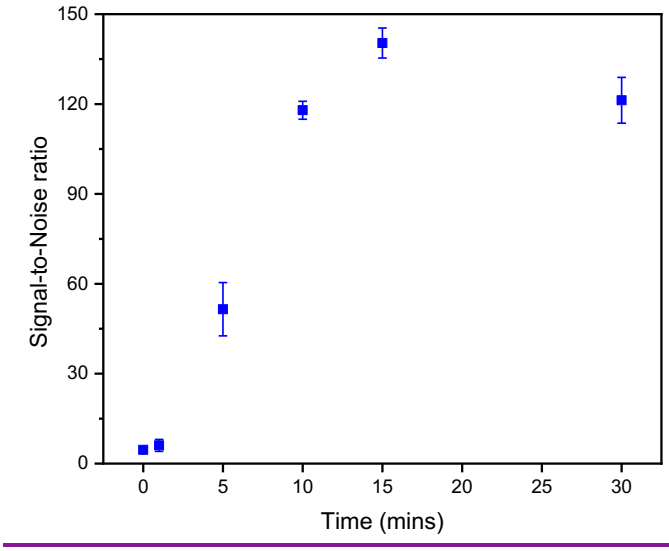

Fig. S2. The silver deposition was tested in the function of time. The concentration of the mixture is 1 mM. The error bars represent the standard deviation of triple measurement.

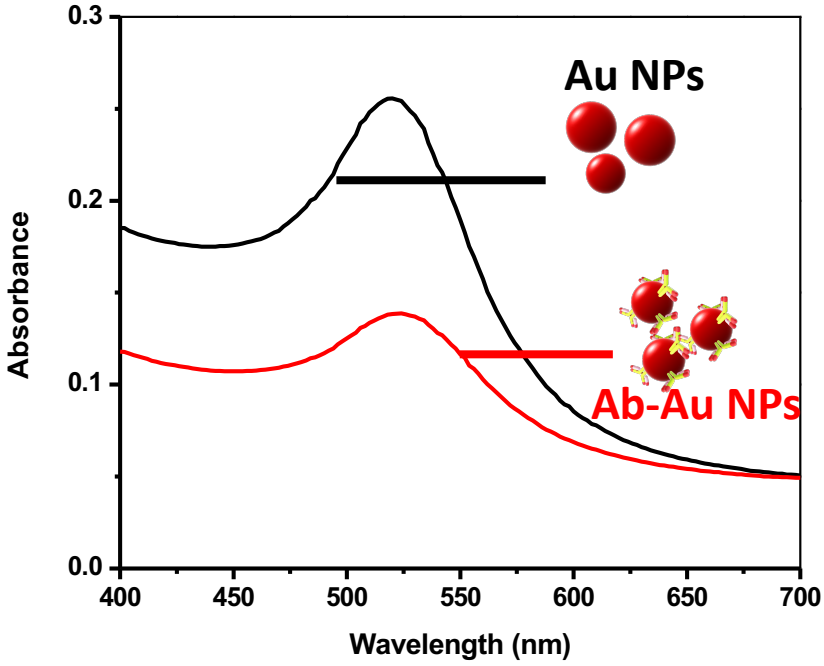

Fig. S3. Absorbance spectrum of AuNPs and Ab-AuNPs.

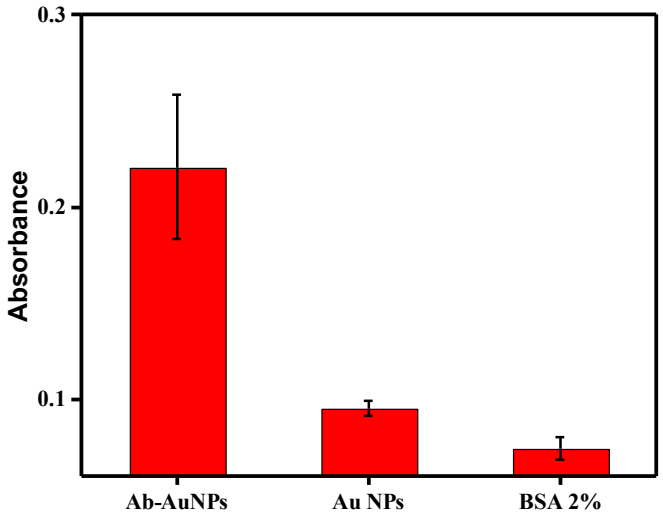

Fig. S4. ELISA for bioconjugation confirmation of anti-HEV Ab/AuNPs. The error bars represent the standard deviation of triple measurements.

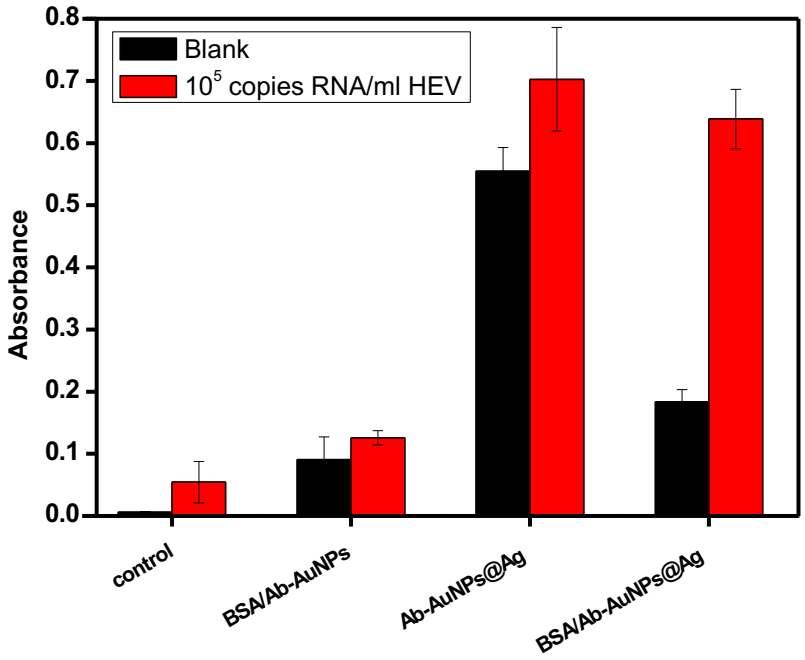

Fig. S5. Influence of BSA-blocking on Au nanoprobes in the matrix sample. The error bars represent the standard deviation of triple measurements,

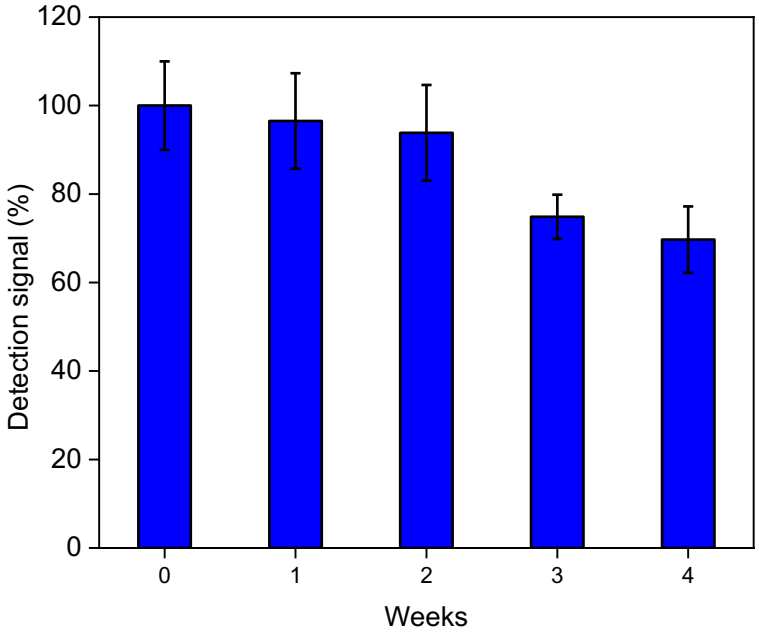

Fig. S6. Stability test of the proposed capture immunoassay. The stability test was done for 4 weeks to detect 10 ng/ml HEV-LPs in buffer. Ab-AuNPs was stored in 4°C throughout the test. The error bars represent the standard deviation of triple measurement.

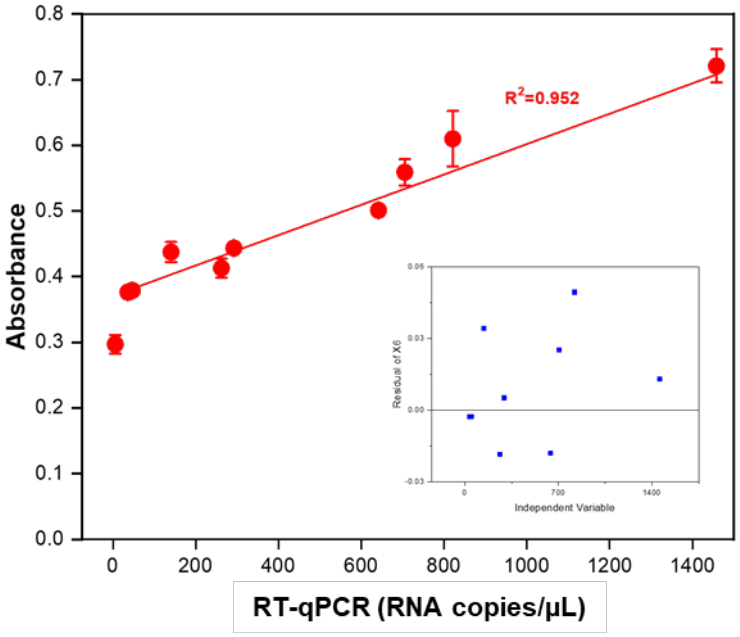

Fig. S7. The signal correlation of proposed capture immunoassay (in absorbance) and RT-qPCR for the monitoring purpose of fecal HEV from stool sample of monkey. The error bars represent the standard deviation of triple measurements. (inset graph showed the residual plot on the linear fit function).